User Guide
Class3Dp 1.0

Authors:

Juan Pedro Carbonell Rivera

Research Technician {juacarri@upv.es}

Dr. Luis Ángel Ruiz Fernández

Professor at Universitat Politècnica de València {laruiz@cgf.upv.es}

Dr. Javier Estornell Cremades

Professor at Universitat Politècnica de València {jaescre@cgf.upv.es}

Content

Introduction

Class3Dp is a software tool developed for supervised classification of photogrammetric point clouds. It allows the selection of training samples and classification of point clouds according to different features and machine learning models. Point clouds obtained from photogrammetric algorithms (e.g., Structure from Motion) include spectral information recorded in the image acquisition process using RGB, multispectral or hyperspectral sensors. The software extracts spectral and geometric features from the point clouds to be used for point classification.

How to use *Class3Dp*

Installation, requirements and execution

Download *Class3Dp* from [http://cgat.webs.upv.es/software/], then unzip it into the selected directory. The software is distributed as a portable version. To execute *Class3Dp*, click on the file Class3Dp.exe and, automatically, the graphical user interface of the software will be displayed.

Input data

The input data required vary according to the processes the user wants to execute. Two possible input data are:

- Photogrammetric point cloud obtained from RGB images in ".las" format, versions 1.2 and 1.3.
- Photogrammetric point cloud obtained from multispectral images (.txt).

The use of different file formats depends on the bands contained in the point cloud. The ".las" format only supports 3 wavelengths, being mostly used by the red (R), green (G) and blue (B) bands. For classifying multispectral point clouds, the user must enter as input a .txt file containing the columns (Figure 1):

- X: Coordinate X.
- Y: Coordinate Y.
- Z: Coordinate Z.
- Blue: Blue band digital number stored in 8 or 16 bits.
- Green: Green band digital number stored in 8 or 16 bits.
- Red: Red band digital number stored in 8 or 16 bits.

- RedEdge: RedEdge band digital number stored in 8 or 16 bits.
- NIR: NIR band digital number stored in 8 or 16 bits.

X	Y	Z	blue	green	red	RedEdge	NIR
649641.145	4746291.551	1521.079	3574.0	2376.0	2110.0	1656.0	959.0
649641.313	4746291.148	1521.091	3480.0	2282.0	2045.0	1589.0	935.0
649640.746	4746291.383	1521.083	3290.0	2185.0	1912.0	1548.0	908.0
649640.895	4746291.004	1521.093	3831.0	2722.0	2521.0	2148.0	1334.0
649640.629	4746291.117	1521.081	3525.0	2439.0	2123.0	1793.0	1083.0

Figure 1. Display of multispectral point cloud data in ".txt" format.

The delimiter value of entry "txt" files is the space. These files must not contain headers. "txt" is a standard output file format for photogrammetric software (e.g., Agisoft Metashape). Currently, with regard to the classification of multispectral point clouds, the software only allows the classification of multispectral point clouds composed of 5 bands (blue, green, red, red edge and near-infrared).

Output data

For point clouds in ".las" format, the classification result is stored in the "Classification" field of the input file. Whereas in the case of point clouds in ".txt" format, the result is stored in a new column of the input file, located last. The result of both classifications are integers, whose values are related to the order previously assigned in the training sample.

Graphical User Interface

The graphical user interface consists mainly of a menu bar and a toolbar. In the menu bar, options File and Help are available:

- File: allows loading or closing the point clouds to be classified.
- Help: provides some help to the user on how to use the software.

The toolbar is divided into 3 tabs Samples, RGB Classification and MS Classification:

- Samples: Selection of training samples from the input point cloud.
- RGB Classification: classification of an RGB point cloud.
- MS Classification: classification of a multispectral point cloud.
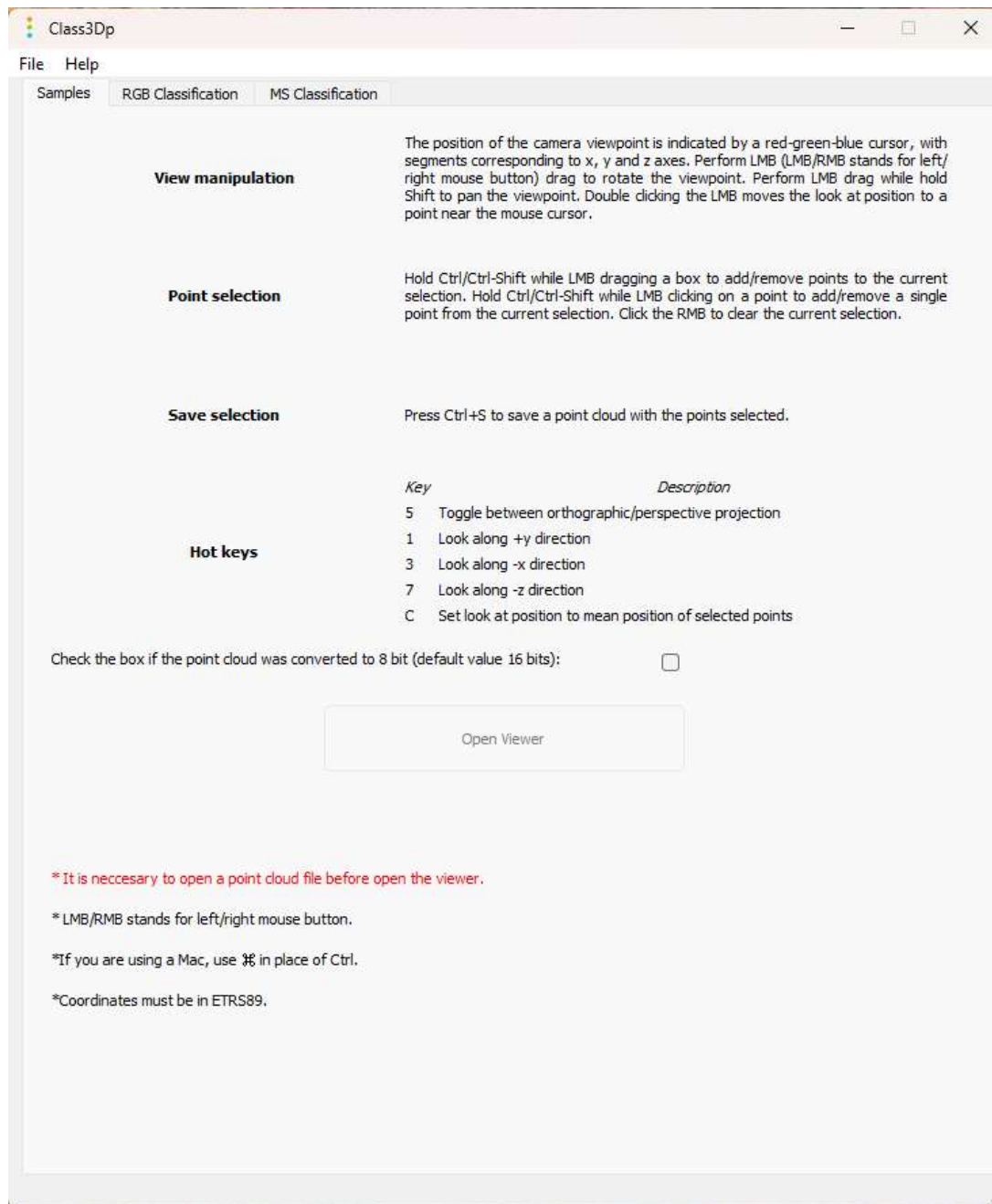
Figure 2. Main window of the Class3Dp software.

1. Samples

In the "Samples" tab (Figure 2), there is a small box with instructions on how to control the 3D viewer. To start the viewer, the user must select a point cloud using "File / Open" from the menu bar. Clicking on the "Open" option will open a selection window, in which ".las" (RGB point clouds) or ".txt" (multispectral point clouds) files can be selected. After selecting a RGB point cloud, press the "Open Viewer" button, which is enabled once the point cloud is loaded. In the case of multispectral point clouds, a new window is shown, in which the user can select the channels to be displayed, as well as the enhance value, which multiplies the values of the digital

levels of the points. The values of the loaded multispectral point cloud are displayed in (Figure 3). As in the case of RGB point clouds, the user must click on the "Open Viewer" button to view the point cloud.
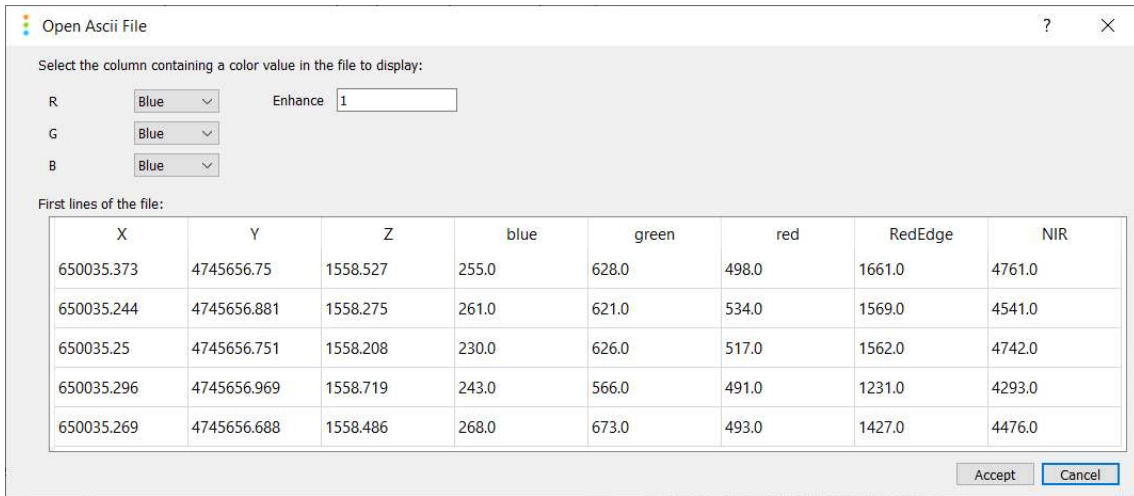
Figure 3. Multispectral point cloud channel selection window.

Once the "Open Viewer" button is pressed, the point cloud starts loading, which may take a few seconds depending on the size of the file. At the end of the loading process, the point cloud is displayed in the viewer (Figure 4).

Figure 4. Class3Dp software visualising a point cloud of 41.7 million points.

The controls for selecting training samples are detailed below (Table 1):

Table 1. Controls for handling the point cloud viewer.

View manipulation	The position of the camera viewpoint is indicated by a red-green-blue cursor, with segments corresponding to x, y and z axes. Perform LMB (LMB/RMB stands for left/right mouse button) drag to rotate the viewpoint. Perform LMB drag while hold Shift to pan the viewpoint. Double clicking the LMB moves the look at position to a point near the mouse cursor.

4

Point selection	Hold Ctrl/Ctrl-Shift while LMB dragging a box to add/remove points to the current selection. Hold Ctrl/Ctrl-Shift while LMB clicking on a point to add/remove a single point from the current selection. Click the RMB to clear the current selection.
Save selection	Press Ctrl+S to save a point cloud with the points selected.
Hot keys	Key Description 5 Toggle between orthographic/perspective projection 1 Look along +y direction 3 Look along -x direction 7 Look along -z direction C Set look at position to mean position of selected points

For the classification of the point cloud, the training samples must be saved in separate files for each class. That is, there will be as many files as classes to be classified. Once the training samples of a class have been saved, the user must delete the selection (RMB), and continue with the selection of new samples.

The files containing the training samples must be in ".las" format in the case of classifying RGB point clouds, and in ".txt" format in the case of classifying multispectral point clouds.

Currently the *Class3Dp* point cloud viewer only supports point clouds in UTM (Universal Transverse Mercator) coordinate system.

2.   RGB Classification

The "RGB Classification" tab (Figure 5) allows the user to perform the classification of a point cloud from training samples of different classes previously selected. First, the user must select the number of classes. Depending on the number of classes, different options will be enabled to select the paths where the ".las" files containing the training samples for each class are located. Similarly, the user will have to select the point cloud to be classified.

Five different machine learning methods are available for classification (Decision Tree (Breiman et al., 1984), Extra Trees (Geurts et al., 2006), MultiLayer Perceptron (Hinton, 1990), Gradient Boosting (Friedman, 2001) and Random Forest (Breiman, 2001)). These classification methods are obtained from the Sklearn library. In addition, a method called "Automatic selection" has been included. This last option performs an adjustment using the 5 different methods described above. Automatically, it chooses the model with the highest cross-validation score (Refaeilzadeh et al., 2009). During the execution of the classification, a console will appear with the status of the process.
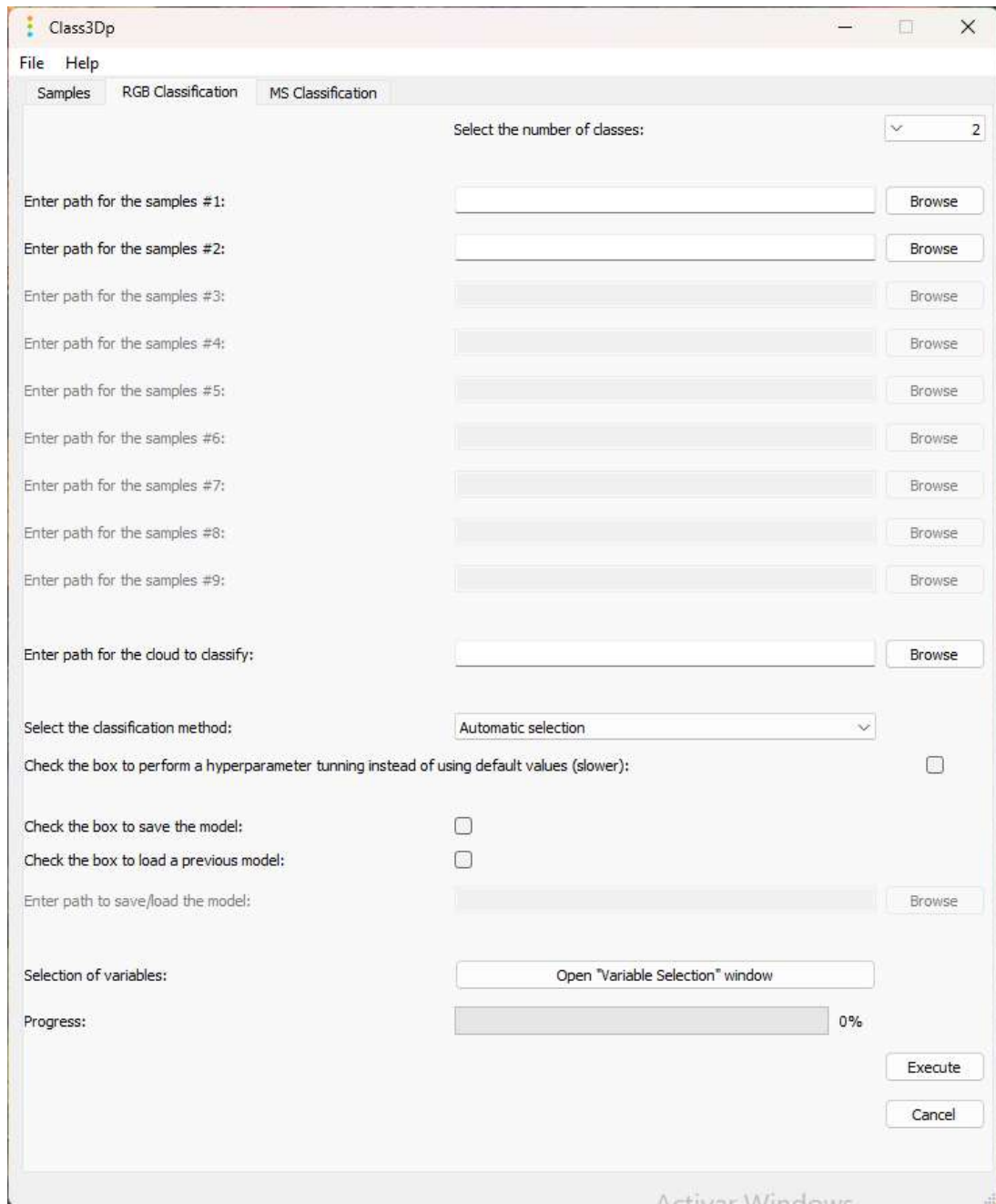
Figure 5. "RGB Classification" tab window.

Within this window, a search can be performed for the best hyperparameters that match the classification method selected by the user, in case this box is not checked, default parameters are taken. The hyperparameters to be evaluated can be seen in Table 2

Table 2. Hyperparameters used in the models' fine-tuning.

Model	Hyperparameter #1 (values)	Hyperparameter #2 (values)	Hyperparameter #3 (values)	Hyperparameter #4 (values)

Decision Tree Extra Trees Gradient Boosting	Maximum depth of the tree (5, 10, None)	Minimum number of samples required to split an internal node (2, 3, 5)	Minimum number of samples required to be at a leaf node (1, 2, 5)	-
Random Forest	Number of trees in the forest (200, 500)	Number of features to consider ('auto', 'sqrt', 'log2')	Maximum depth of the tree (4, 5, 6, 7, 8)	Function to measure the quality of a split ('gini', 'entropy')
MultiLayer Perceptron	Number of neurons in the ith hidden layer (50,50,50), (50,100,50), (100)	Activation ('tanh', 'relu')	Solver ('sgd', 'adam')	Alpha (0.0001, 0.05)

The calculated model can be saved by selecting the checkbox "Check the box to save the model". This allows to reuse the model later. The loading of a previously saved model is done in a similar way. For the correct loading of the model, the user must select the same features used to generate the model. To do this, use the window "Feature Selection", then the features can be selected and introduced into the model. The available features are shown in table 3.

Table 3. Features used in the RGB classification.

Type	Name (Description)	Equation	Reference
Geometrical	Coordinate X of the point	X	-
Geometrical	Coordinate Y of the point	Y	-
Geometrical	Height of the point	Z	-
Spectral	Blue value of the point	Blue	-
Spectral	Green value of the point	Green	-
Spectral	Red value of the point	Red	-
Spectral	BI (Brightness)	$\rho_{red} + \rho_{green} + \rho_{blue}$	(Fraser et al., 2017)
Spectral	CIVE (Color Index of Vegetation)	$0.441 * \rho_{red} - 0.881 * \rho_{green} + 0.385 * \rho_{blue} + 18.78745$	(Kataoka et al., 2003)
Spectral	EXG (Index Excess Green Minus Excess Red)	$(2 * \rho_{green} - \rho_{red} - \rho_{blue}) - (1.4 * \rho_{red} - \rho_{green)}$	(Neto, 2004)
Spectral	ExG (Index Excess Green)	$(2 * \rho_{green} - \rho_{red} - \rho_{blue})$	(Woebbecke et al., 1995)
Spectral	GLI (Green Leaf Index)	$(2 * \rho_{green} - \rho_{red} - \rho_{blue})/(2 * \rho_{green} + \rho_{red} + \rho_{blue})$	(Vala & Baxi, 2013)
Spectral	GR (Green divided by red)	ρ_{green}/ρ_{red}	(Fraser et al., 2017)
Spectral	MGVRI (Modified Green-Red Vegetation Index)	$(\rho_{green}^2 - \rho_{red}^2)/(\rho_{green}^2 + \rho_{red}^2)$	(Barbosa et al., 2019)
Spectral	NBRDI (Normalised Blue-Red Difference Index)	$(\rho_{red} - \rho_{blue})/(\rho_{red} + \rho_{blue})$	(Carbonell-Rivera et al., 2020)
Spectral	NGBDI (Normalised Green-Blue Difference Index)	$(\rho_{green} - \rho_{blue})/(\rho_{green} + \rho_{blue})$	(Shimada et al., 2012)
Spectral	NGRDI (Normalised Green-Red Difference Index)	$(\rho_{green} - \rho_{red})/(\rho_{green} + \rho_{red})$	(Hunt et al., 2005)
Spectral	NormG (Normalized Greeness)	$\rho_{green}/(\rho_{green} + \rho_{red} + \rho_{blue})$	(Stricker et al., 2014)

Spectral	RGRI (Red Green Ratio Index)	ρ_{red}/ρ_{green}	(Gamon & Surfus, 1999)
Spectral	SAVI (Soil Adjusted Vegetation Index)	$(1.5 * (\rho_{green} - \rho_{red}))/(\rho_{green} + \rho_{red} + 0.5)$	(A. R. Huete, 1988)
Spectral	VARI (Visual Atmospheric Resistance Index)	$(\rho_{green} - \rho_{red})/(\rho_{green} + \rho_{red} - \rho_{blue})$	(Gitelson et al., 2002)
Spectral	vNDVI (Visible Normalized Difference Vegetation Index)	$0.5268 * \rho_{red}^{-0.1294} * \rho_{green}^{0.3389} * \rho_{blue}^{-0.3118}$	(Costa et al., 2020)
Neighbourhood	Numbers (Number of neighbours)	n	-
Neighbourhood spectral	NGRDI_mean (Mean NGRDI of the point and its neighbouring points)	$\overline{\text{NGRDI}}(S_p) = \frac{1}{n}\left(\sum_{i=1}^{n} \text{NGRDI}(S_{p,i})\right)$	-
Neighbourhood spectral	NGRDI_std (Standard deviation NGRDI of the point and its neighbouring points)	$\sqrt{\frac{(\sum_{i=1}^{n}(\text{NGRDI}(S_{p,i}) - \overline{\text{NGRDI}}(S_p))^2)}{n-1}}$	-
Neighbourhood Geometrical	Dist_mean (Mean distance of the point with its neighbouring points)	$\bar{d}(S_p, p) = \frac{1}{n}\left(\sum_{i=1}^{n} d(S_{p,i}, p)\right)$	-
Neighbourhood Geometrical	Dist_std (Standard deviation of the point with its neighbouring points)	$\sqrt{\frac{[(\sum_{i=1}^{n}(d(S_{p,i}, p) - \bar{d}(S_p, p))^2)]/(n-1)}{n-1}}$	-
Neighbourhood geometrical	Z_mean (Mean height of the point and its neighbours)	$\bar{z}(S_p) = \frac{1}{n}\left(\sum_{i=1}^{n}(z(S_{p,i})\right)$	-
Neighbourhood geometrical	Z_std (Standard deviation height of the point and its neighbours)	$\sqrt{\frac{(\sum_{i=1}^{n}(z(S_{p,i}) - \bar{z}(S_p))^2)}{n-1}}$	-
Neighbourhood geometrical	Dif_Z (Maximum height of the neighbourhood minus minimum height of the neighbourhood)	$\max(z(S_p)) - \min(z(S_p))$	-
Neighbourhood geometrical	Z_Zmin (Height of the point minus neighbourhood minimum height)	$z(p) - \min(z(S_p))$	-
Neighbourhood geometrical	Zmax-Z (Maximum height of the neighbourhood minus height of the point)	$\max(z(S_p)) - z(p)$	-
Neighbourhood geometrical	Sum_λ (Sum of eigenvalues)	$\lambda_1 + \lambda_2 + \lambda_3$	(Rusu, 2010)
Neighbourhood geometrical	Omnivariance	$\sqrt[3]{\lambda_1 \cdot \lambda_2 \cdot \lambda_3}$	(West et al., 2004)
Neighbourhood geometrical	Eigenentropy	$-\sum_{i=1}^{3} \lambda_i \cdot \ln(\lambda_1)$	(West et al., 2004)
Neighbourhood geometrical	Anisotropy	$(\lambda_1 - \lambda_3)/\lambda_1$	(West et al., 2004)
Neighbourhood geometrical	Planarity	$(\lambda_2 - \lambda_3)/\lambda_1$	(West et al., 2004)
Neighbourhood geometrical	Linearity	$(\lambda_1 - \lambda_2)/\lambda_1$	(West et al., 2004)
Neighbourhood geometrical	Surface Variation	$\lambda_3/(\lambda_1 + \lambda_2 + \lambda_3)$	(Rusu, 2010)
Neighbourhood geometrical	Sphericity	λ_3/λ_1	(West et al., 2004)
Neighbourhood geometrical	Verticality	1-nz	(Demantké et al., 2012)

Once the training samples are selected, the point cloud to classify is added, and the classification method and the features have been selected, the user can click on the "Execute" button and the classification process starts. During the execution, the user can visualize at any time information of the process being carried out (calculation of the variables, model adjustment or classification of the point cloud from the calculated model).

After determining the classification model, for the evaluation of the model, the mean cross-validation score and the cross-validation score of each fold are displayed. Likewise, the confusion matrix obtained from the evaluation of the learning samples in the adjusted model is shown. In addition, the permutation importance (Breiman, 2001) obtained by each feature in the classification is displayed. This information can be used for the user to perform a dimensional reduction.

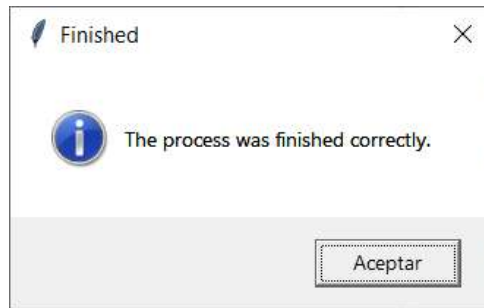If the process has been successfully completed a new window is displayed (Figure 6).

Figure 6. Process completion window.

3. MS Classification

The multispectral classification shows a very similar window as the RGB classification. The main differences are the use of ".txt" files in the point clouds and the selection of new features derived from the additional bands used in this format (NIR and Rededge). The features that can be calculated are shown in table 4.

Table 4. Features used in the multispectral classification.

Type	Name (Description)	Equation	Reference
Geometrical	Coordinate X of the point	X	-
Geometrical	Coordinate Y of the point	Y	-
Geometrical	Height of the point	Z	-
Spectral	Blue value of the point	Blue	-
Spectral	Green value of the point	Green	-
Spectral	Red value of the point	Red	-

Spectral	RedEdge value of the point	RedEdge	-
Spectral	NIR value of the point	NIR	-
Spectral	ARVI (Atmospherically Resistant Vegetation Index)	$(\rho_{nir} - \rho_{rb})/(\rho_{nir} + \rho_{rb})$, $\rho_{rb} = \rho_{red} - [\rho_{blue} - \rho_{red}/2]$	(Kaufman & Tanre, 1992)
Spectral	BI (Brightness)	$\rho_{green} + \rho_{red} + \rho_{blue}$	(Fraser et al., 2017)
Spectral	DVI (Differential Vegetation Index)	$\rho_{nir} - \rho_{red}$	(Richardson & Wiegand, 1977)
Spectral	EVI (Enhanced Vegetation Index)	$[2.5 \cdot (\rho_{blue} - \rho_{red})]/[(\rho_{nir} + 6 \cdot \rho_{red} - 7.5 \cdot \rho_{blue} + 1)]$	(A. Huete et al., 1999)
Spectral	GNDVI (Green Normalised Difference Vegetation Index)	$(\rho_{nir} - \rho_{green})/(\rho_{nir} + \rho_{green})$	(Gitelson et al., 1996)
Spectral	GR (Green divided by red)	ρ_{green}/ρ_{red}	(Fraser et al., 2017)
Spectral	IPVI (Infrared Percentage Vegetation Index)	$\rho_{nir}/(\rho_{nir} + \rho_{green})$	(Ray et al., 1993)
Spectral	MSAVI (Modified Soil-Adjusted Vegetation Index)	$(2 \cdot \rho_{nir} + 1 - [(2 \cdot \rho_{nir} + 1)^2 - 8 \cdot (\rho_{nir} - \rho_{red})]^{0.5})/2$	(Qi et al., 1994)
Spectral	MSR (Modified Simple Ratio Index)	$\rho_{red}/(\rho_{nir}/\rho_{red})^{0.5}$	(Chen, 1996)
Spectral	NDVI (Normalised Difference Vegetation Index)	$(\rho_{nir} - \rho_{red})/(\rho_{nir} + \rho_{red})$	(Rouse et al., 1974)
Spectral	NBRDI (Normalised Blue-Red Difference Index)	$(\rho_{red} - \rho_{blue})/(\rho_{red} + \rho_{blue})$	(Carbonell-Rivera et al., 2020)
Spectral	NGBDI (Normalised Green-Blue Difference Index)	$(\rho_{green} - \rho_{blue})/(\rho_{green} + \rho_{blue})$	(Shimada et al., 2012)
Spectral	NGRDI (Normalised Green-Red Difference Index)	$(\rho_{green} - \rho_{red})/(\rho_{green} + \rho_{red})$	(Hunt et al., 2005)
Spectral	NormG (Normalised Greenness)	$\rho_{green}/(\rho_{green} + \rho_{red} + \rho_{blue})$	(Stricker et al., 2014)
Spectral	OSAVI (Optimised Soil Adjusted Vegetation Index)	$(\rho_{nir} - \rho_{red})/(\rho_{nir} + \rho_{red} + 0.16)$	(Rondeaux et al., 1996)
Spectral	RDVI (Renormalised Difference Vegetation Index)	$(\rho_{nir} - \rho_{red})/(\rho_{nir} + \rho_{red})^{0.5}$	(Roujean & Breon, 1995)
Spectral	RGRI (Red Green Ratio Index)	ρ_{red}/ρ_{green}	(Gamon & Surfus, 1999)
Spectral	RVI (Ratio Vegetation Index)	ρ_{red}/ρ_{nir}	(Jordan, 1969)
Spectral	SARVI (Soil and Atmospherically Resistant Vegetation Index)	$[1.5 \cdot (\rho_{nir} - \rho_{rb})]/(\rho_{nir} + \rho_{red} + 0.5)$, $\rho_{rb} = \rho_{red} - [\rho_{blue} - \rho_{red}/2]$	(A. R. Huete, 1988)
Spectral	SAVI (Soil Adjusted Vegetation Index)	$1.5 \cdot (\rho_{nir} - \rho_{rb})/(\rho_{nir} + \rho_{red} + 0.5)$	(A. R. Huete, 1988)
Spectral	SR (Simple Ration Vegetation Index)	ρ_{nir}/ρ_{red}	(Tucker, 1979)
Spectral	SRxNDVI (Simple Ratio × Normalised Difference Vegetation Index)	$(\rho_{nir}^2 - \rho_{red})/(\rho_{nir} + \rho_{red}^2)$	(Gong et al., 2003)
Neighbourhood	Numbers (Number of neighbours)	n	-
Neighbourhood spectral	NDVI_mean (Mean NDVI of the point and its neighbouring points)	$\overline{NDVI}(S_p) = \frac{1}{n}\left(\sum_{i=1}^{n} NDVI(S_{p,i})\right)$	-
Neighbourhood spectral	NDVI_std (Standard deviation NDVI of the point and its neighbouring points)	$\sqrt{\frac{(\sum_{i=1}^{n}(NDVI(S_{p,i}) - \overline{NDVI}(S_p))^2)}{n-1}}$	-
Neighbourhood geometrical	Dist_mean (Mean distance of the point with its neighbouring points)	$\bar{d}(S_p, p) = \frac{1}{n}\left(\sum_{i=1}^{n} d(S_{p,i}, p)\right)$	-
Neighbourhood geometrical	Dist_std (Standard deviation of the point with its neighbouring points)	$\sqrt{\frac{(\sum_{i=1}^{n}(d(S_{p,i}, p) - \bar{d}(S_p, p))^2)}{n-1}}$	-

Neighbourhood geometrical	Z_mean (Mean height of the point and its neighbours)	$\bar{z}(S_p) = \frac{1}{n}\left(\sum_{i=1}^{n}(z(S_{p,i}))\right)$	-
Neighbourhood geometrical	Z_std (Standard deviation height of the point and its neighbours)	$\sqrt{\dfrac{(\sum_{i=1}^{n}(z(S_{p,i}) - \bar{z}(S_p))^2)}{n-1}}$	-
Neighbourhood geometrical	Dif_Z (Maximum height of the neighbourhood minus minimum height of the neighbourhood)	$\max(z(S_p)) - \min(z(S_p))$	-
Neighbourhood geometrical	Z_Zmin (Height of the point minus neighbourhood minimum height)	$z(p) - \min(z(S_p))$	-
Neighbourhood geometrical	Zmax-Z (Maximum height of the neighbourhood minus height of the point)	$\max(z(S_p)) - z(p)$	-
Neighbourhood geometrical	Sum_λ (Sum of eigenvalues)	$\lambda_1 + \lambda_2 + \lambda_3$	(Rusu, 2010)
Neighbourhood geometrical	Omnivariance	$\sqrt[3]{\lambda_1 \cdot \lambda_2 \cdot \lambda_3}$	(West et al., 2004)
Neighbourhood geometrical	Eigenentropy	$-\sum_{i=1}^{3}\lambda_i \cdot \ln(\lambda_1)$	(West et al., 2004)
Neighbourhood geometrical	Anisotropy	$(\lambda_1 - \lambda_3)/\lambda_1$	(West et al., 2004)
Neighbourhood geometrical	Planarity	$(\lambda_2 - \lambda_3)/\lambda_1$	(West et al., 2004)
Neighbourhood geometrical	Linearity	$(\lambda_1 - \lambda_2)/\lambda_1$	(West et al., 2004)
Neighbourhood geometrical	Surface Variation	$\lambda_3/(\lambda_1 + \lambda_2 + \lambda_3)$	(Rusu, 2010)
Neighbourhood geometrical	Sphericity	λ_3/λ_1	(West et al., 2004)
Neighbourhood geometrical	Verticality	1-nz	(Demantké et al., 2012)

Software tips

This manual is accompanied by a video tutorial in which an example of point cloud classification is visualized, performing a classification with two classes, bare ground points and vegetation. The point cloud used in this tutorial is attached to be used for software testing purposes.

Execution of several *Class3Dp* processes

If the user wants to execute several *Class3Dp* processes, run the Classes.exe file as many times as desired.

Error output

Any error raised while executing will be showed in the Log and/or saved in file "Filelog.log", located in the main directory of *Class3Dp*.

Python libraries used

All the python libraries used for the development of *Class3Dp* are:

- Joblib (https://pypi.org/project/joblib/)
- Keyboard (https://pypi.org/project/keyboard/)
- Laspy (https://pypi.org/project/laspy/)
- Logging (https://docs.python.org/3/library/logging/)
- numpy (https://pypi.org/project/numpy/)
- os (https://docs.python.org/3/library/os.html)
- pandas (https://pypi.org/project/pandas/)
- pptk (https://pypi.org/project/pptk/)
- PyQt5 (https://pypi.org/project/PyQt5/)
- Scipy (https://pypi.org/project/scipy/)
- Scikit-learn (https://scikit-learn.org/)
- sys (https://docs.python.org/3/library/sys.html)
- tkinter (https://docs.python.org/3/library/tkinter.html)
- traceback (https://docs.python.org/3/library/traceback.html)

License

This software is released under Attribution-NonCommercial-ShareAlike 4.0 International (CC BY-NC-SA 4.0). More information can be found in the license.md file that accompanies the software.

References

Barbosa, B. D. S., Ferraz, G. A. S., Gonçalves, L. M., Marin, D. B., Maciel, D. T., Ferraz, P. F. P., & Rossi, G. (2019). RGB vegetation indices applied to grass monitoring: a qualitative analysis. *Agronomy Research*, *17*(2), 349–357. https://doi.org/10.15159/AR.19.119

Breiman, L. (2001). Random forests. *Machine Learning*, *45*(1), 5–32.

Breiman, L., Friedman, J., Stone, C. J., & Olshen, R. A. (1984). *Classification and regression trees*. CRC press.

Carbonell-Rivera, J. P., Estornell, J., Ruiz, L. A., Torralba, J., & Crespo-Peremarch, P. (2020). Classification of UAV-based photogrammetric point clouds of riverine species using machine learning algorithms: A case study in the Palancia river, Spain. *The International Archives of the Photogrammetry, Remote Sensing and Spatial Information Sciences*, *XLIII-B2-2020*(B2), 659–666. https://doi.org/10.5194/ISPRS-ARCHIVES-XLIII-B2-2020-659-2020

Chen, J. M. (1996). Evaluation of vegetation indices and a modified simple ratio for boreal applications. *Canadian Journal of Remote Sensing*, *22*(3), 229–242.

Costa, L., Nunes, L., & Ampatzidis, Y. (2020). A new visible band index (vNDVI) for estimating NDVI values on RGB images utilizing genetic algorithms. *Computers and Electronics in Agriculture*, *172*, 105334. https://doi.org/10.1016/J.COMPAG.2020.105334

Demantké, J., Vallet, B., & Paparoditis, N. (2012). Streamed vertical rectangle detection in terrestrial laser scans for facade database production. *ISPRS Annals of the Photogrammetry, Remote Sensing and Spatial Information Sciences*, *I–3*, 99–104. https://doi.org/10.5194/ISPRSANNALS-I-3-99-2012

Fraser, R. H., van der Sluijs, J., & Hall, R. J. (2017). Calibrating Satellite-Based Indices of Burn Severity from UAV-Derived Metrics of a Burned Boreal Forest in NWT, Canada. *Remote Sensing 2017, Vol. 9, Page 279*, *9*(3), 279. https://doi.org/10.3390/RS9030279

Friedman, J. H. (2001). Greedy function approximation: A gradient boosting machine. *Annals of Statistics*, *29*(5), 1189–1232. https://doi.org/10.1214/AOS/1013203451

Gamon, J. A., & Surfus, J. S. (1999). Assessing leaf pigment content and activity with a reflectometer. *The New Phytologist*, *143*(1), 105–117. https://doi.org/10.1046/J.1469-8137.1999.00424.X

Geurts, P., Ernst, D., & Wehenkel, L. (2006). Extremely randomized trees. *Machine Learning*, *63*(1), 3–42.

Gitelson, A. A., Kaufman, Y. J., & Merzlyak, M. N. (1996). Use of a green channel in remote sensing of global vegetation from EOS-MODIS. *Remote Sensing of Environment*, *58*(3), 289–298.

Gitelson, A. A., Kaufman, Y. J., Stark, R., & Rundquist, D. (2002). Novel algorithms for remote estimation of vegetation fraction. *Remote Sensing of Environment*, *80*(1), 76–87. https://doi.org/10.1016/S0034-4257(01)00289-9

Gong, P., Pu, R., Biging, G. S., & Larrieu, M. R. (2003). Estimation of forest leaf area index using vegetation indices derived from Hyperion hyperspectral data. *IEEE Transactions on Geoscience and Remote Sensing*, *41*(6), 1355–1362.

Hinton, G. (1990). Connectionist learning procedures. *Machine Learning*. https://www.sciencedirect.com/science/article/pii/B9780080510552500298

Huete, A., Justice, C., & van Leeuwen, W. (1999). MODIS vegetation index (MOD13). *Algorithm Theoretical Basis Document*, *3*(213), 295–309.

Huete, A. R. (1988). A soil-adjusted vegetation index (SAVI). *Remote Sensing of Environment*, *25*(3), 295–309.

Hunt, E. R., Cavigelli, M., Daughtry, C. S. T., Mcmurtrey, J. E., & Walthall, C. L. (2005). Evaluation of digital photography from model aircraft for remote sensing of crop biomass and nitrogen status. *Precision Agriculture*, *6*(4), 359–378.

Jordan, C. F. (1969). Derivation of leaf-area index from quality of light on the forest floor. *Ecology*, *50*(4), 663–666.

Kataoka, T., Kaneko, T., Okamoto, H., & Hata, S. (2003). Crop growth estimation system using machine vision. *Proceedings 2003 IEEE/ASME International Conference on Advanced*

Intelligent Mechatronics (AIM 2003), *2*, b1079-b1083 vol.2. https://doi.org/10.1109/AIM.2003.1225492

Kaufman, Y. J., & Tanre, D. (1992). Atmospherically resistant vegetation index (ARVI) for EOS-MODIS. *IEEE Transactions on Geoscience and Remote Sensing*, *30*(2), 261–270.

Neto, J. C. (2004). A combined statistical-soft computing approach for classification and mapping weed species in minimum -tillage systems. *ETD Collection for University of Nebraska - Lincoln*. https://digitalcommons.unl.edu/dissertations/AAI3147135

Qi, J., Chehbouni, A., Huete, A. R., Kerr, Y. H., & Sorooshian, S. (1994). A modified soil adjusted vegetation index. *Remote Sensing of Environment*, *48*(2), 119–126.

Ray, T. W., Farr, T. G., Blom, R. G., & Crippen, R. E. (1993). *Monitoring land use and degradation using satellite and airborne data*.

Refaeilzadeh, P., Tang, L., & Liu, H. (2009). Cross-Validation. *Encyclopedia of Database Systems*, 532–538. https://doi.org/10.1007/978-0-387-39940-9_565

Richardson, A. J., & Wiegand, C. L. (1977). Distinguishing vegetation from soil background information. *Photogrammetric Engineering and Remote Sensing*, *43*(12), 1541–1552.

Rondeaux, G., Steven, M., & Baret, F. (1996). Optimization of soil-adjusted vegetation indices. *Remote Sensing of Environment*, *55*(2), 95–107.

Roujean, J.-L., & Breon, F.-M. (1995). Estimating PAR absorbed by vegetation from bidirectional reflectance measurements. *Remote Sensing of Environment*, *51*(3), 375–384.

Rouse, J. W., Haas, R. H., Schell, J. A., Deering, D. W., & Harlan, J. C. (1974). Monitoring the vernal advancement and retrogradation (green wave effect) of natural vegetation. *NASA/GSFC Type III Final Report, Greenbelt, Md*, *371*.

Rusu, R. B. (2010). Semantic 3D Object Maps for Everyday Manipulation in Human Living Environments. *KI - Künstliche Intelligenz 2010 24:4*, *24*(4), 345–348. https://doi.org/10.1007/S13218-010-0059-6

Shimada, S., Matsumoto, J., Sekiyama, A., Aosier, B., & Yokohana, M. (2012). A new spectral index to detect Poaceae grass abundance in Mongolian grasslands. *Advances in Space Research*, *50*(9), 1266–1273. https://doi.org/10.1016/J.ASR.2012.07.001

Stricker, R., Müller, S., & Gross, H.-M. (2014). Non-contact video-based pulse rate measurement on a mobile service robot. *The 23rd IEEE International Symposium on Robot and Human Interactive Communication*, 1056–1062.

Tucker, C. J. (1979). Red and photographic infrared linear combinations for monitoring vegetation. *Remote Sensing of Environment*, *8*(2), 127–150.

Vala, H. J., & Baxi, A. (2013). *A Review on Otsu Image Segmentation Algorithm*.

West, K. F., Webb, B. N., Lersch, J. R., Pothier, S., Triscari, J. M., & Iverson, A. E. (2004). Context-driven automated target detection in 3D data. *Https://Doi.Org/10.1117/12.542536*, *5426*, 133–143. https://doi.org/10.1117/12.542536

Woebbecke, D. M., Meyer, G. E., von Bargen, K., & Mortensen, D. A. (1995). Color Indices for Weed Identification Under Various Soil, Residue, and Lighting Conditions. *Transactions of the ASAE*, *38*(1), 259–269. https://doi.org/10.13031/2013.27838